MHD FLOW AND THERMAL ANALYSIS OF WATER-BASED NANOFLUIDS WITH COPPER (Cu) AND ALUMINUM OXIDE (Al2O3) NANOPARTICLES: AN ADVANCED FRACTIONAL APPROACH

Kaouther GHACHEM[1], Khurram JAVID[2], Sami ULLAH KHAN[3], Imen SAFRA[1], Hind ALBALAWI[4], Lioua KOLSI[5]

[1]Department of Industrial Engineering and Systems, College of Engineering, Princess Nourah bint Abdulrahman University, P.O. Box 84428, Riyadh 11671, Saudi Arabia, (imsafra@pnu.edu.sa, kgmaatki@pnu.edu.sa)

[2]Department of Mathematics, Northern University, Wattar-Wallai Road, Nowshera, 24110, KPK, Pakistan

(khurram_javid1985@yahoo.com)

[3]Department of Mathematics, Namal University, Mianwali 42250, Pakistan (sk_iiu@yahoo.com)

[4]Department of Physics, College of Sciences, Princess Nourah bint Abdulrahman University, P.O. Box 84428, Riyadh, 11671, Saudi Arabia

[5]Department of Mechanical Engineering, College of Engineering, University of Ha'il, Ha'il City, Saudi Arabia

(lioua_enim@yahoo.fr)

[*]**Correspondence:** sk_iiu@yahoo.com

Abstract: *Owing to improved thermal features, the hybrid nanomaterials present multidisciplinary applications in thermal systems, extrusion processes, solar energy, engineering processes, chemical reaction etc. Following such impressive applications in mind, the aim of current work is to present the heat transfer analysis for free convective flow of hybrid nanofluid due to two parallel plates. The hybrid nanofluid is based on utilization of copper (Cu) and aluminum oxide (Al2O3) nanoparticles with water base fluid. The motivations for considering the copper (Cu) and aluminum oxide (Al2O3) nanoparticles are due to high thermal accuracy. The fractional simulations are performed with help of Prabhakar fractional technique. The Prabhakar fractional derivative is more effective as it provides more flexible and comprehensive framework for modelling the complex systems with memory features hereditary features and anomalous diffusion. The integration process is subject to implementation of Laplace technique. It has been claimed that the improvement in volumetric fraction leads to reduction of fluid velocity. The temperature profile reduces due to higher Prandtl number and control of heat transfer is more impressive for copper base hybrid nanofluid.*

Keywords: *Prabhakar fractional model; nanofluid; mixed convection flow; heat transfer, Parallel Plates.*

1. Introduction

Channel flows play a significant role in various industrial processes, including within chemical reactors, heat exchangers and the broader field of thermal engineering [1]. The phenomenon of natural convection fluid flows is crucial for scientists and engineers, given its extensive application in several sectors. These include solar collectors, fiber insulation, cooling processes for electronic devices and geothermal energy systems [2]. The study and application of free convective flow, especially in configurations limited by parallel surfaces, has attracted attention due to its relevance in many engineering scenarios. Research efforts, such as those of Singh et al. [3], looked at transient natural convection patterns observed between parallel plates, improving our understanding of such phenomena. Similarly, investigations of Riga surface flow have been extended to include nanoparticles in the context of mass diffusion and constant temperature environments, as explored by Shafiq et al. [4]. Marneni et al. [5] focused on the dynamics of natural convective flow between two plates under a ramp wall condition, contributing valuable insights into the control and manipulation of these flows.

Magnetohydrodynamics (MHD) flows have also captivated the interest of the scientific and engineering communities due to their applicability in various fields, including electronic transformers, MHD accelerators, and freezing processes of metal plates in freezing baths. [5]. The study of MHD convective flows, involving different fluids and geometric configurations, has been a significant area of research, highlighting the diverse potential of MHD applications. Despite extensive research on magnetohydrodynamics (MHD) natural convection flows in channels, the exploration of free convection in electrically conductive fluids within such configurations is less common. Jha et al. [6] addressed this gap by examining natural convection and fully developed flow with MHD effect in a plate channel. Reddy et al. [7] conducted thermo-diffusion insight to Casson fluid under the influence of magnetic force. Cham et al. [8] predicted the unsteady flow of Casson fluid with applications of magnetohydrodynamics effects. Fwaz et al. [9] visualized the response of magnetic force for nanofluid with parametric effects. The significance of electrically conducting material over permeable vertical surface has been analyzed by Bhargavi et al. [10].

The concept of nanofluid have attracted the interest of researchers due to superior heat transfer capabilities. Recent studies have highlighted that NFs outperform traditional fluids in terms of heat exchange efficiency, suggesting their potential to replace conventional fluids in various applications. Owing to outstanding thermal properties have attracted attention in various fields such as transportation, nuclear power, electronics, biomedicine and the food industry. The unique thermal effects of nanoparticles mixed with base fluids have been recognized [11]. Reddy et al. [12] carefully explored the effects of a micropolar model combining heat flow with magnesium oxide nanoparticles. Hassan et al. discussed how the viscosity of a nanofluid changes under high shear conditions [13]. Balan et al. [14] detected the heat transfer in double pipe flow of nanofluid with heat exchanger application. Bouzid et al. [15] contributed to analyzing enhancement of heat transfer in cavity filled with hybrid nanofluid for mixed convection flow. Khedher et al. [16] addressed the turbulence analysis in Casson nanofluid problem by following the Stokes transformation. Hussain et al. [17] executed the contribution of nanoparticles radius in analyzing optimized thermal performances of dusty fluid due to stretched surface.

Hybrid Nanofluids (HNFs), which consist of a combination of different nanoparticles in base fluids, have shown significant effects on heat transfer and fluid dynamics. Khan et al. [18] discussed the thermal results due to gyrating sphere by entertaining the blood based hybrid nanofluid. Waini et al. [19] examined the onset of mixed convection in porous media containing various nanoparticles. The study of MHD free convection of HNFs in a porous medium using the finite element method was conducted by Babazadeh et al. [20]. Asadi et al. [21] proposed the influence of UFHs on the efficiency of the system. Huminic et al. [22] explored various thermal structures under different boundary and physical conditions to understand their effects on entropy generation in nanofluids (NFs) and hybrid nanofluids (HNFs). Nadeem et al. [23] studied the thermal characteristics of HNFs on an exponentially curved surface. Song et al. [24] examined Marangoni convection in hybrid nanofluids with the addition of additional heating sources. The behavior of Williamson nanofluid around a stretched cylinder, influenced by mixed convection, was detailed by Song et al. [25]. Kumar et al. [26] analyzed the dynamics of dust particles in the presence of hybrid nanoparticles, employing a modified heat flux approach. Prasannakumara [27] studied the influence of magnetic dipoles on the flow of Maxwell nanofluids on stretched surfaces. Nagapavani et al. [28] focused on the thermal effects of carbon nanotubes (CNTs) combined with various nanoparticles. Mahanthesh's [29] research was on hybrid nanofluids using C2H6O2-H2O as the base fluid. Mackolil and Mahanthesh [30] studied the thermal behavior of copper nanoparticles in conjunction with polar particles. Sheikholeslami [31] focused on the thermal dynamics nanofluid, considering solar energy applications. Mezaache et al. [32] analyzed thermal impact of nanofluid flow in wavy channel.

The field of fractional calculus has seen the application of various fractional derivatives, including those named after Marchand, Grünwald-Letnikov, Hadamard, Riesz and Caputo [34, 35]. Turkyilmazoglu [36] developed the fractional model for cancerous tumor in breast. Ibraheem et al. [37] performed the analytical simulations of fractional order differential equations with implementation of optimal variational iteration scheme. Turkyilmazoglu and Altanji [38] performed the analytical simulations via Caputo derivative for free falling bodies subject to both linear and quadratic fractional forces. Sene [39] explored the second-grade fractional model using the Caputo-Liouville operator. Mozafarifard and Toghraie [40] used the Caputo method to study the behavior of thin metal sheets. In various fractional techniques, the Prabhakar fractional derivative is most effective and advanced analytical tool to solve various complex differential equations. The application of Prabhakar's fractional derivative led to the development of generalized constitutive laws, obviating the need for a fractional flow model between two plates. Prabhakar's fractional operator, notable for its three-parameter kernel and its reliance on the widely recognized Mittag-Leffler function, has proven effective in deriving mathematical models for practical problems. Research involving analytical simulations using the Prabhakar integral and its properties has been extensive [41-44]. Giusti and Colombaro [45] introduced a generalized model for non-Newtonian flow, based on fractional calculus and generalized constitutive principles, with the kernel of the Prabhakar derivative playing a crucial role in managing the heating layers. Akgül et al. [46] investigated magnetohydrodynamic (MHD) effects on convective heat transfer, while Wang et al. [47] studied the flow of Casson nanofluids using an improved Mittag-Leffler kernel technique. Additional advances and research regarding the Mittag-Leffler function have been documented [48-50].

In the current study, we introduce a fractional model to study the mixed convection of MHD flows of nanofluids between two parallel plates, incorporating mass transfer effects. Our focus is on improving heat transfer achievable through the dispersion of copper or aluminum oxide nanoparticles in a water-based fluid, under the influence of an external magnetic field. A steady buoyancy driven flow of nanofluid is considered which is essential in nuclear reactor, cooling systems and solar collectors. The innovative aspect of our model lies in its application of fractional order derivatives according to recent advances, specifically by employing Prabhakar's fractional calculus to simulate these effects. This approach allows us to take into account the memory characteristics inherent to the fractional model. Although various fractional models have been proposed to address nanofluid dynamics, the specific scenario of MHD nanofluid flow subject to both heat and mass transfer influences, as modeled by Prabhakar's fractional calculation, has not been explored previously. The proposed mathematical formulation aims to fill this research gap. The study systematically examines the impact of various parameters on flow behavior, presenting the results through graphical illustrations.

2. Problem description

This research delves into the dynamic characteristics of nanofluid flow that is incompressible and confined between two parallel plates separated by a fixed distance d, as illustrated in Figure 1. Initially, both the fluid and the system find themselves in equilibrium. However, as time advances from the initial moment ($t>0^+$), motion is induced in one of the plates due to the application of time-dependent shear stress. Simultaneously, the nanofluid is propelled between the permeable plates by the synergistic influence of vibrational forces and the ambient thermal conditions. Furthermore, an external magnetic field, aligned at an angle θ relative to the direction of the flow, is imposed. The development of the flow model takes into account a set of fundamental assumptions:

- The flow is unsteady and caused by the motion of the plate.
- The surfaces of plates are porous.
- The constant temperature and concentration are defined as T_d and C_d .
- The magnetic force is applied normally to the plates.

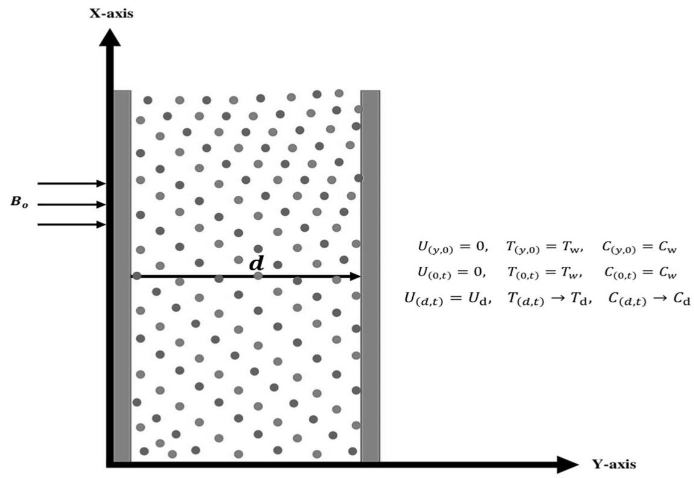

Figure 1: Considered geometry with boundary conditions.

In view of these considered assumptions, the developed model is expressed as [41-43]:

$$\rho_{nf}\frac{\partial U_{(y,t)}}{\partial t} = \mu_{nf}\frac{\partial^2 U_{(y,t)}}{\partial y^2} - \left(\sigma_{nf}B_o^2 sin(\theta) + \frac{\mu_{nf}\varphi_{nf}}{K}\right)U_{(y,t)} + g(\beta_T)_{nf}\left(T_{(y,t)} - T_{\mathrm{d}}\right) + g(\beta_C)_{nf}\left(C_{(y,t)} - C_{\mathrm{d}}\right), \tag{1}$$

$$\left(\rho C_p\right)_{nf}\frac{\partial T_{(y,t)}}{\partial t} = -\frac{\partial \delta_{(y,t)}}{\partial y}, \qquad \delta_{(y,t)} = -k_{nf}\frac{\partial T_{(y,t)}}{\partial y}, \tag{2}$$

$$\frac{\partial C_{(y,t)}}{\partial t} = -\frac{\partial J_{(y,t)}}{\partial y}, \qquad J_{(y,t)} = -D\frac{\partial C_{(y,t)}}{\partial y}. \tag{3}$$

The dimensional boundary conditions are:

$$U_{(y,0)} = 0, \quad T_{(y,0)} = T_{\mathrm{w}}, \quad C_{(y,0)} = C_{\mathrm{w}}; \quad \forall y \geq 0 \tag{4}$$

$$U_{(0,t)} = 0, \quad T_{(0,t)} = T_w, \quad C_{(0,t)} = C_w; \quad y = 0 \tag{5}$$

$$U_{(d,t)} = U_{\mathrm{d}}, \quad T_{(d,t)} \to T_{\mathrm{d}}, \quad C_{(d,t)} \to C_{\mathrm{d}}; \quad t > 0 \tag{6}$$

The following dimensionless variables [41, 42]:

$$U^* = \frac{d}{\nu_f}U,\ t^* = \frac{\nu t}{d^2},\quad t_o = \frac{\nu}{U_o^2},\quad y^* = \frac{\mathrm{y}}{d},\quad T^* = \frac{T_{(y,t)} - T_{\mathrm{d}}}{T_w - T_{\mathrm{d}}},\quad \delta^* = \delta_o$$

$$C^* = \frac{C_{(y,t)} - C_{\mathrm{d}}}{C_{\mathrm{w}} - C_{\mathrm{d}}}$$

are used to establish the dimensionless form of the governing equations:

$$\frac{\partial U_{(y,t)}}{\partial t} = \frac{\partial^2 U_{(y,t)}}{\partial y^2} - \left(Msin(\theta) + K_{eff}\right)U_{(y,t)} + T_{(y,t)} + NC_{(y,t)}, \tag{7}$$

$$Pr\frac{\partial T_{(y,t)}}{\partial t} = -\frac{\partial \delta_{(y,t)}}{\partial y}, \qquad \delta_{(y,t)} = -\frac{\partial T_{(y,t)}}{\partial y} \tag{8}$$

$$Sc\frac{\partial C_{(y,t)}}{\partial t} = -\frac{\partial J_{(y,t)}}{\partial y}, \qquad J_{(y,t)} = -\frac{\partial C_{(y,t)}}{\partial y}. \tag{9}$$

with

$$\mathrm{Sc} = \frac{\nu}{D}, \quad M = \frac{\sigma^* k B_o^2}{\mathrm{h}^2 \mu}, \quad Gr = \frac{g\beta_T d^3 (T_\mathrm{w} - T_\mathrm{d})}{\nu^2}$$

$$K_{eff} = \frac{\nu\,\varphi_1}{K^* U_o^2}, \qquad Pr = \frac{\nu_f C_p}{k}, \qquad \mathrm{N} = \frac{\mathrm{Gm}}{Gr}, \qquad Gm = \frac{g\beta_C (C_\mathrm{w} - C_\mathrm{d}) d^3}{\nu^2}$$

The dimensionless boundary conditions are:

$$U_{(y,0)} = 0, \qquad T_{(y,0)} = 0, \qquad C_{(y,0)} = 0; \qquad \forall y \geq 0 \tag{10}$$

$$U_{(0,t)} = 0, \qquad T_{(0,t)} = 0, \qquad C_{(0,t)} = 0\,; \qquad y = 0 \tag{11}$$

$$U_{(1,t)} = 1, \quad T_{(1,t)} = 1, \qquad C_{(1,t)} = 0; \qquad t > 0 \tag{12}$$

Table 1 presents the expressions used to evaluate of the properties of the nanofluid. Table 2 illustrates the nanoparticles and base fluid properties.

Table 1: Relations used to evaluate the nanofluid properties [29, 30].

Property	Nanofluid
Density	$\rho_f = \dfrac{\rho_{nf}}{(1-\varphi) + \varphi\dfrac{\rho_s}{\rho_s}}$
Dynamic Viscosity	$\mu_f = \mu_{nf}(1-\varphi)^{2.5}$
Electrical conductivity	$\sigma_f = \dfrac{\sigma_{nf}}{\left(1 + \dfrac{3\left(\frac{\sigma_s}{\sigma_f} - 1\right)\varphi}{\left(\frac{\sigma_s}{\sigma_f} + 2\right) - \left(\frac{\sigma_s}{\sigma_f} - 1\right)\varphi}\right)}$
Thermal conductivity	$k_f = \dfrac{k_{nf}}{\left(\dfrac{k_s + (n-1)k_f - (n-1)(k_f - k_s)\varphi}{k_s + (n-1)k_f + (k_f - k_s)\varphi}\right)}$
Heat capacitance	$(\rho C_p)_f = \dfrac{(\rho C_p)_{nf}}{(1-\varphi) + \varphi\dfrac{(\rho C_p)_s}{(\rho C_p)_f}}$
Thermal Expansion Coefficient	$(\rho\beta)_f = \dfrac{(\rho\beta)_{nf}}{(1-\varphi) + \varphi\dfrac{(\rho\beta)_s}{(\rho\beta)_f}}$

Table 2: Thermal impact of nanoparticles and water [29-30].

Material	H_2O	Al_2O_3	Cu
$\rho(\mathrm{kg/m^3})$	997.1	3970	8933
$\mathrm{C_p(J/kg\ K)}$	4179	765	385
$\mathrm{k(W/m\ K)}$	0.613	40	401
$\beta_\mathrm{T} \times 10^{-5}(\mathrm{K^{-1}})$	21	1.67	1.67
$\beta_\mathrm{C} \times 10^{-5}(\mathrm{K^{-1}})$	298.2	4.05	3.05

3. Prabhakar scheme

The Prabhakar scheme defined over continuous function $h(t)$ with some operator ${}^{C}\mathfrak{D}^{\gamma}_{\alpha,\beta,\alpha}$ is defined as:

$${}^{C}\mathfrak{D}^{\gamma}_{\alpha,\beta,\alpha}h(t) = E^{-\gamma}_{\alpha,m-\beta,\alpha}h^{m}(t) = \int_0^t (t-\tau)^{m-\beta-1} E^{-\gamma}_{\alpha,m-\beta}(\alpha(t-\tau)^{\alpha})h^{m}(\tau)d(\tau),$$

Where:

$$E^{\gamma}_{\alpha,\beta,\alpha}\mathrm{h}(t) = \int_0^t (t-\tau)^{\beta-1} E^{\gamma}_{\alpha,\beta}(\alpha(t-\tau)^{\alpha})\mathrm{h}(\tau)d(\tau),$$

$$E^{\gamma}_{\alpha,\beta}(z) = \sum_{n=0}^{\infty}\frac{\Gamma(\gamma+n)z^{n}}{n!\,\Gamma(\gamma)\Gamma(\alpha n+\beta)'}, \qquad \alpha,\beta,\gamma\epsilon\mathbb{C}, \quad Re(\alpha)>0$$

$$\mathcal{L}\left\{{}^{C}\mathfrak{D}^{\gamma}_{\alpha,\beta,\alpha}h(t)\right\} = q^{\beta-m}(1-\alpha q^{-\alpha})^{\gamma}\mathcal{L}\{h^{m}(t)\}, \tag{13}$$

$$\delta_{(y,t)} = -{}^{C}\mathfrak{D}^{\gamma}_{\alpha,\beta,\alpha}\frac{\partial T_{(y,t)}}{\partial y} \tag{14}$$

$$J_{(y,t)} = -{}^{C}\mathfrak{D}^{\gamma}_{\alpha,\beta,\alpha}\frac{\partial C_{(y,t)}}{\partial y} \tag{15}$$

4. Simulations of the problem

Under the physical assumptions outlined, this section is devoted to formulating the governing equations using the Prabhakar fractional approach, as well as to the development of corresponding fractional solutions.

Concentration profile:

$$Sc\ q\ \bar{C}_{(y,q)} = -\frac{\partial \bar{J}_{(y,q)}}{\partial y} \tag{16}$$

$$\bar{J}_{(y,q)} = -q^{\beta}(1-\alpha q^{-\alpha})^{\gamma}\frac{\partial \bar{C}_{(\xi,q)}}{\partial y} \tag{17}$$

With: $\bar{C}_{(0,q)} = 0, \bar{C}_{(1,q)} = \frac{1}{q}$.

$$\bar{C}_{(y,q)} = \frac{1}{q}\frac{Sinh\left(y\sqrt{\frac{Sc\ q^{1-\beta}}{(1-\alpha q^{-\alpha})^{\gamma}}}\right)}{Sinh\left(\sqrt{\frac{Sc\ q^{1-\beta}}{(1-\alpha q^{-\alpha})^{\gamma}}}\right)} \tag{18}$$

Temperature profile

Applying fractional operator on heat equation:

$$Pr\ q\bar{T}_{(y,q)} = -\frac{\partial \bar{\delta}_{(y,q)}}{\partial y} \tag{19}$$

$$\bar{\delta}_{(y,q)} = -q^{\beta}(1-\alpha q^{-\alpha})^{\gamma}\frac{\partial \bar{T}_{(y,q)}}{\partial y} \tag{20}$$

with $\bar{T}_{(0,q)} = 0,\ \ \bar{T}_{(1,q)} = \frac{1}{q}$.

$$\bar{T}_{(y,q)} = \frac{1}{\mathrm{q}}\frac{Sinh\left(y\sqrt{\frac{Pr_{eff}\ q^{1-\beta}}{(1-\alpha q^{-\alpha})^{\gamma}}}\right)}{Sinh\left(\sqrt{\frac{Pr_{eff}\ q^{1-\beta}}{(1-\alpha q^{-\alpha})^{\gamma}}}\right)} \tag{21}$$

Solution of the velocity field

$$q\,\bar{U}_{(y,q)} = \frac{\partial^2 \bar{U}_{(y,q)}}{\partial y^2} - \left(M\sin(\theta) + K_{eff}\right)\bar{U}_{(y,q)} + \bar{T}_{(y,q)} + N\bar{C}_{(y,q)}, \tag{22}$$

with conditions

$\bar{U}_{(0,q)} = 0; \qquad \bar{U}_{(y,q)} = \frac{1}{q}.$

$$\bar{U}_{(y,q)} = \frac{e^{y\sqrt{(MSin(\theta)+K_{eff}+q)}} - e^{-y\sqrt{(MSin(\theta)+K_{eff}+q)}}}{e^{\sqrt{(MSin(\theta)+K_{eff}+q)}} - e^{-\sqrt{(MSin(\theta)+K_{eff}+q)}}}\left(\frac{1}{q}\frac{1}{\frac{Pr_{eff}\,q^{1-\beta}}{(1-\alpha q^{-\alpha})^{\gamma}} - \left(MSin(\theta) + K_{eff} + q\right)} + \frac{1}{q}\frac{1}{\frac{Sc\,q^{1-\beta}}{(1-\alpha q^{-\alpha})^{\gamma}} - \left(MSin(\theta) + K_{eff} + q\right)}\right)$$
$$- \frac{1}{q}\frac{1}{\frac{Pr_{eff}\,q^{1-\beta}}{(1-\alpha q^{-\alpha})^{\gamma}} - \left(MSin(\theta) + K_{eff} + q\right)}\frac{e^{y\sqrt{\frac{Pr_{eff}\,q^{1-\beta}}{(1-\alpha q^{-\alpha})^{\gamma}}}} - e^{-y\sqrt{\frac{Pr_{eff}\,q^{1-\beta}}{(1-\alpha q^{-\alpha})^{\gamma}}}}}{e^{\sqrt{\frac{Pr_{eff}\,q^{1-\beta}}{(1-\alpha q^{-\alpha})^{\gamma}}}} - e^{-\sqrt{\frac{Pr_{eff}\,q^{1-\beta}}{(1-\alpha q^{-\alpha})^{\gamma}}}}}$$
$$+ \frac{1}{q}\frac{1}{\frac{Sc\,q^{1-\beta}}{(1-\alpha q^{-\alpha})^{\gamma}} - \left(MSin(\theta) + K_{eff} + q\right)}\frac{e^{y\sqrt{\frac{Sc\,q^{1-\beta}}{(1-\alpha q^{-\alpha})^{\gamma}}}} - e^{-y\sqrt{\frac{Sc\,q^{1-\beta}}{(1-\alpha q^{-\alpha})^{\gamma}}}}}{e^{\sqrt{\frac{Sc\,q^{1-\beta}}{(1-\alpha q^{-\alpha})^{\gamma}}}} - e^{-\sqrt{\frac{Sc\,q^{1-\beta}}{(1-\alpha q^{-\alpha})^{\gamma}}}}} \tag{23}$$

$$U(y,t) = \frac{ln(2)}{t}\sum_{n=1}^{N} v_n \bar{U}\left(y, n\frac{ln(2)}{t}\right),$$

$$v_n = (-1)^{n+\frac{N}{2}} \sum_{r=\left[\frac{q+1}{2}\right]}^{min\left(q,\frac{N}{2}\right)} \frac{r^{\frac{N}{2}}(2r)!}{\left(\frac{N}{2} - r\right)!\,r!\;(r-1)!\;(q-r)!\;(2r-q)!},$$

and

$U(y,t) = \frac{e^{4.7}}{t}\left[\frac{1}{2}\bar{U}\left(r, \frac{4.7}{t}\right) + Re\left\{\sum_{j=1}^{N}(-1)^k \bar{U}\left(r, \frac{4.7+k\pi i}{t}\right)\right\}\right].$

5. Results and Discussion

This research explores the behavior of mixed convection flows involving viscous and incompressible nanofluids, specifically Cu-water and Al_2O_3-water nanofluids, as they navigate between two parallel plates. The study delves into heat and mass transfer processes influenced by an external magnetic field. A novel fractional model has been introduced, utilizing a contemporary interpretation of fractional operators that encapsulate memory effects, specifically through the Prabhakar fractional derivative. This model is addressed using the Laplace Transform method. The influence of key parameters on the flow dynamics and the associated heat and mass transfer characteristics are depicted and analyzed through graphical presentations. The modeled problem is subject to theoretical flow assumptions, therefore, graphical computations are performed for specific range of flow parameters like $0.1 \le \alpha \le 0.9$, $0.1 \le \beta \le 0.9, 4.5 \le Pr \le 7.5$, $2.4 \le Sc \le 3.9$, $0.01 \le \varphi \le 0.04$, $0.1 \le N \le 1.5$, $0.75 \le M \le 2.25$ and $0.4 \le t \le 1.4$.

Figure 2(a-b) illustrates how the Prandtl number and fractional parameters (α, β, γ) influence the thermal profile. Figure 2(a) displays the temperature profiles for the two considered types of nanofluids, across the dimensionless spatial variable y. for various values of the fractional parameters α, β and γ. The curves for Cu-nanofluid are higher than those for Al_2O_3-nnofluid, indicating that Cu nanoparticles result in a higher temperature at the same distance from the heat source, due to the higher thermal conductivity of Cu compared to Al_2O_3. As the fractional parameters increase, the temperature profile flattens out for both types of nanofluids, indicating, the effectiveness of heat transfer through the fluid decreases and the profile becomes more uniform across the y axis. Figure 2(b) illustrates the effect of varying Pr on the temperature profile. As Pr increases, the temperature profiles become steeper, indicating a stronger temperature gradient. This means that for fluids with a higher Pr, the conductive heat transfer is more significant relative to convective transfer. This is due to increased viscosity, which tends to suppress convective flows and enhance the dominance of conduction. The temperature profiles broaden with decreasing Pr, implying that lower Pr values favor convective heat transfer, leading to a more uniform temperature distribution.

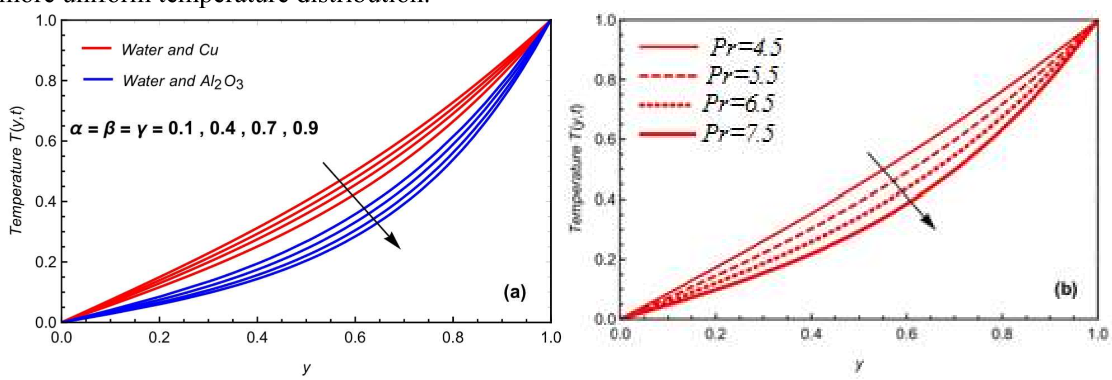

Figure 2(a-b): Effects of (a) fractional parameters and (b) Pr values on the temperature profile.

Figure 3(a-b) displays the effects of fractional parameters α, β and γ and the Schmidt number Sc on the concentration profile for the considered nanofluids. As presented in Figure 3(a), for both types of nanofluids, as α, β and γ increase, the concentration profiles become less steep, indicating a more uniform distribution of the concentration across the distance y. This is due to enhanced diffusion effects as the fractional parameters increase. The curves for Cu-nanofluid are higher than those for Al_2O_3-nanofluid, suggesting that the Cu nanoparticles help achieving higher concentrations more quickly. Figure 3(b) illustrates the impact of varying the Schmidt number Sc on the concentration profile. The Schmidt number is a dimensionless number that describes the ratio of momentum diffusivity to mass diffusivity. As the Schmidt number increases, the concentration profiles become steeper. This suggests that with higher Sc values, the diffusion of mass is slower relative to the momentum transfer, leading to a sharper gradient in concentration. The steepest concentration profile occurs at $Sc = 3.9$, which suggests that at this value, the mass diffusivity is relatively low compared to the viscosity of the fluid, resulting in a concentration that changes more abruptly with the distance. As the Schmidt number decreases, the concentration gradient becomes less steep, implying that lower Sc values favor mass diffusion.

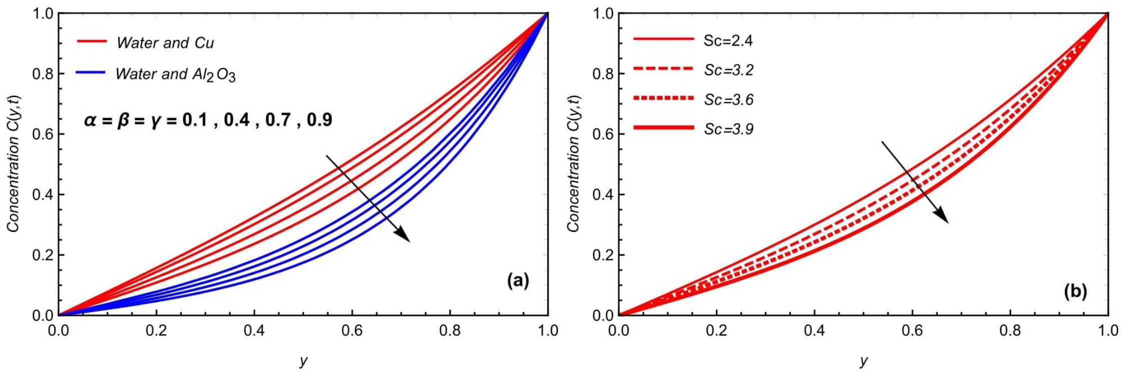

Figure 3(a-b): Effects of (a) fractional parameters and (b) Schmidt number on the concentration profile.

Figure 4(a-b) depicts the effects of fractional parameters and nanoparticles volume fraction on the velocity profiles for fixed values of Pr, Sc, M, N and t. Figure 4(a) illustrates how the fractional parameters α, β and γ affect the velocity profile. The graph shows that as $\alpha = \beta = \gamma$ increase, the peak velocity of the fluid decreases for both types of nanofluids. This suggests that higher fractional parameters are associated with greater fluid resistance, which affects the momentum diffusion. The Cu-nanofluid exhibits a higher velocity profile than the Al_2O_3 -nanofluid at the same fractional parameters, which indicates that Cu nanoparticles have a different impact on the fluid's viscosity and hence its flow characteristics. Figure 4(b) displays the impact of varying the nanoparticles volume fraction on the velocity profile. As φ increases, the peak velocity of the fluid seems to decrease slightly for both types of nanofluids. This is due to the increased presence of solid particles within the fluid, which increases the effective viscosity and create more resistance to flow. Both Cu and Al_2O_3 nanofluids show a similar trend with increasing φ, but the Cu-nanofluid consistently shows a higher velocity profile than the Al_2O_3 nanofluid at corresponding volume fractions. This suggests that, while both types of nanoparticles affect the flow, they do so to different extents, due to the differences in their physical properties.

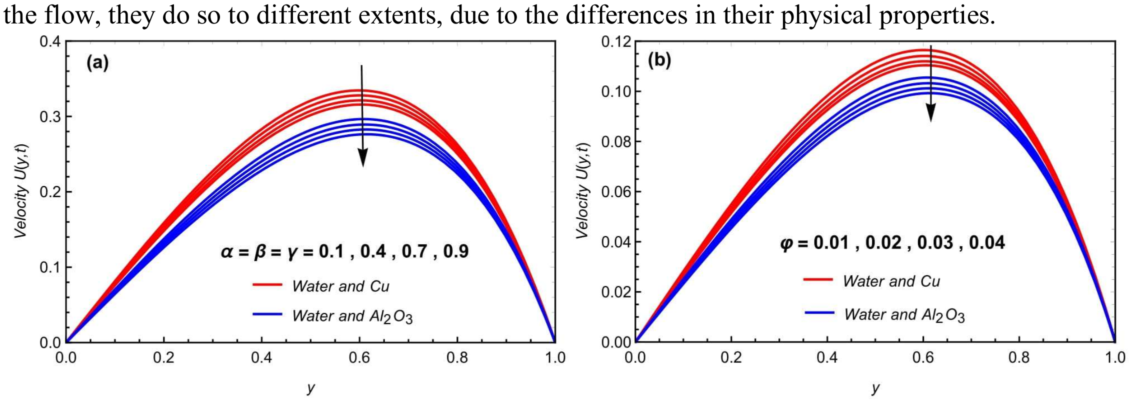

Figure 4(a-b): Effects of (a) fractional parameters and (b) nanoparticles volume fraction on the velocity profile, for $Pr = 7.5,\ Sc = 4.5,\ M = 1.75,\ N = 1.5,\ and\ t = 0.8$

Figure 5(a-b) explores the effects of the magnetic parameter and the buoyancy ratio on the velocity profiles of both of nanofluids under fixed conditions. It is noticed from Figure 5(a) that, as the magnetic parameter increases, the peak velocity within the fluid decreases for both types of nanofluids. This is indicative of the damping effect of a magnetic field on the flow of an electrically conducting fluid. The magnetic field induces a Lorentz force that acts against the motion of the fluid, thus slowing it down. The effect of the magnetic parameter on the Cu nanofluid is more pronounced than on the Al_2O_3 nanofluid, as seen by the more significant decrease in velocity with increasing M. This is because the presence of copper, which is a better electrical conductor than aluminum oxide, makes the fluid more responsive to magnetic fields. Figure 5(b) illustrates the influence of N on the velocity profile. As the buoyancy ratio increases, the peak velocity for both nanofluids increases as well. The buoyancy ratio is the ratio of thermal buoyancy force to solutal buoyancy force, which suggests that thermal effects are becoming more dominant over concentration-based effects. A higher buoyancy ratio enhances natural convection within the nanofluid, which increases the nanofluid velocity due to buoyancy-driven flow. This is consistent with the upward trend in velocity profiles with increasing N. The effect of buoyancy appears to be more pronounced for the Cu nanofluid than for the Al_2O_3 nanofluid, due to the different thermal properties of the two types of nanoparticles.

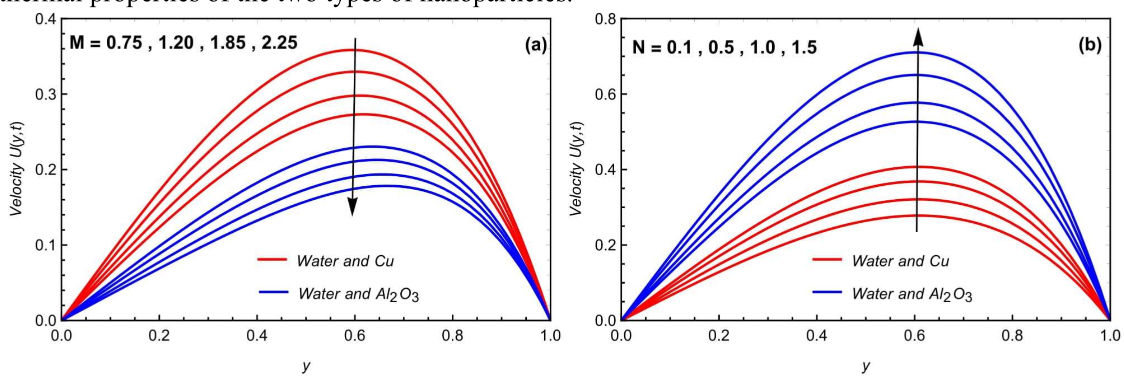

Figure 5(a-b): Effects of (a) Magnetic parameter and (b) buoyancy ratio on the velocity profile, for $\alpha = \beta = \gamma = 0.5,\ Pr = 7.5,\ Sc = 4.5,\ \ \varphi = 0.02,\ and\ t = 0.8$.

Figure 6(a-b) presents the effects of dimensionless time t and the Prandtl number Pr on the velocity profiles of a fluid under certain conditions. Figure 6(a) shows that as the dimensionless time increases, the peak velocity of the fluid decreases. This implies that over time, the system is reaching a more relaxed state, in fact it is approaching a steady state where the influence of initial conditions diminishes. The system is experiencing a deceleration of flow as it evolves over time. This is due to various physical factors, including the increasing influence of viscous forces and, the development of a boundary layer. In Figure 6(b), we see that as the Prandtl number increases, the peak velocity of the fluid increases as well. A higher Prandtl number indicates that thermal diffusivity is low compared to momentum diffusivity. Therefore, for higher Prandtl numbers, the fluid's velocity is less hindered by thermal effects, leading to a higher velocity profile. The trend shows that increasing Pr can lead to enhanced velocity profiles, which is due to the lower thermal conductivity of the fluid at higher Pr numbers, resulting in less energy being lost to heat and more being available to drive the flow.

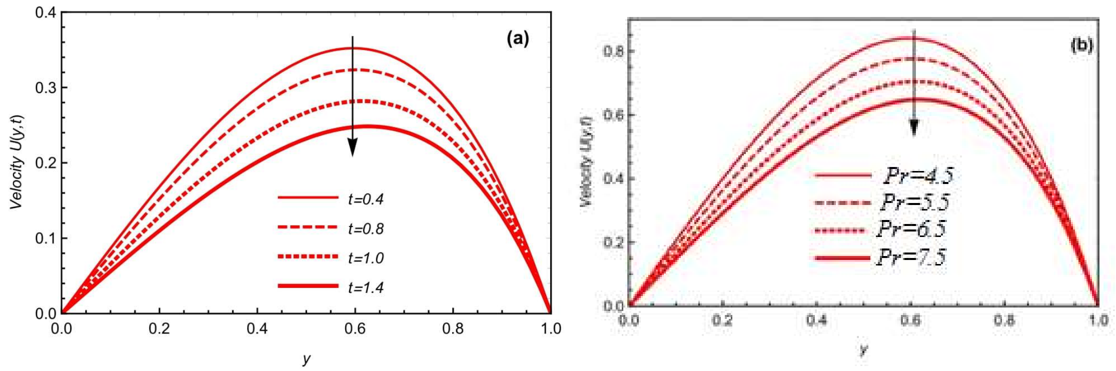

Figure 6(a-b): Effects of (a) dimensionless time and (b) Prandtl number on the velocity profile, for with $\alpha = \beta = \gamma = 0.5,\ Sc = 4.5,\ M = 1.75,\ N = 1.5,\ \varphi = 0.02$.

Figure 7(a-b) investigates the influences of the Schmidt number and the type of nanofluid at different times on the velocity profiles. Figure 7(a) shows that increasing Sc leads to a decrease in the peak velocity for both types of nanofluids. Higher Sc indicates that the fluid's viscosity is more influential compared to the mass diffusion. This higher viscosity results in a slower velocity profile due to increased resistance to flow. The impact of the Schmidt number is noticeable for both types of nanofluids, but Cu-nanofluid consistently shows higher velocity profiles across the range of Sc values, suggesting that the Cu nanoparticles have different impact on the fluid's viscosity than Al_2O_3 nanoparticles. Figure 7(b) claims that concentration declined upon increasing time instant.

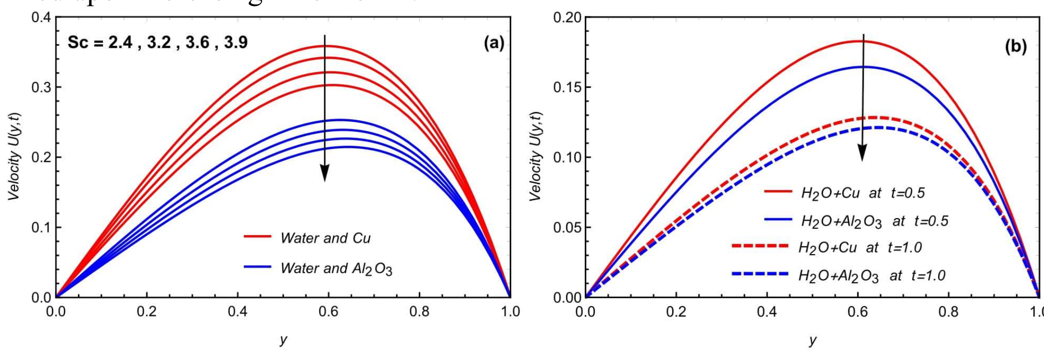

Figure 7(a-b): Effects of (a) Schmidt number and (b) type of nanofluid for various times on the velocity profile.

Table 3 presents the numerical simulations for temperature profile $T_{(y,t)}$, concentration profile $C_{(y,t)}$ and velocity profile $V_{(y,t)}$ at two different time instants $t = 0.5$ and $t = 1.0$. The results are prepared by increasing distance from the inclined plate. The findings reveal that $T_{(y,t)}$, and $C_{(y,t)}$ increases when y increases.

Table 3: Numerical analysis for temperature profile $T_{(y,t)}$, concentration profile $C_{(y,t)}$ and velocity profile $V_{(y,t)}$ at $t = 0.5$ and $t = 1.0$.

	$T_{(y,t)}$		$C_{(y,t)}$		$V_{(y,t)}$	
y	$t = 0.5$	$t = 1.0$	$t = 0.5$	$t = 1.0$	$t = 0.5$	$t = 1.0$
0.1	0.0561	0.0625	0.0194	0.0269	0.0709	0.0579
0.2	0.1146	0.1217	0.0419	0.0567	0.1385	0.1482
0.3	0.1779	0.1959	0.0707	0.0928	0.1994	0.2128
0.4	0.2485	0.2711	0.1098	0.1388	0.2497	0.2656
0.5	0.3294	0.3551	0.1644	0.1996	0.2848	0.3017
0.6	0.4237	0.4506	0.2414	0.2810	0.2993	0.3157
0.7	0.5348	0.5603	0.3501	0.3910	0.2869	0.3012

Table 4 presents the results of Nusselt number (Nu), Sherwood number (Sh) and skin friction coefficient (C_f) subject to variation of fractional parameter α. A comparative analysis is observed for two distinct time intervals t = 0.5 and t = 1.0. A reduction in Nu and Sh has been observed due to higher values of α. However, the both physical quantities maintaining leading values at $\mathrm{t}=1.0$. Similar results are examined for C_f.

Table 4: The Illustration of Sherwood number, Nusselt number and skin friction for fractional parameter α.

Parameter	Nu		Sh		C_f	
α	$\mathrm{t}=0.5$	$t=1.0$	$t=0.5$	$t=1.0$	$t=0.5$	$t=1.0$
0.1	1.2393	1.4339	0.4631	0.7037	1.5022	1.6426
0.2	1.2044	1.3962	0.4344	0.6599	1.4813	1.6213
0.3	1.1703	1.3501	0.4107	0.6143	1.4609	1.5947
0.4	1.1399	1.2982	0.3927	0.5697	1.4429	1.5640
0.5	1.1152	1.2441	0.2802	0.5283	1.4287	1.5319
0.6	1.0739	1.1919	0.3727	0.4920	1.4188	1.5008
0.7	1.0860	1.1451	0.3694	0.4620	1.4130	1.4730
0.8	1.0806	1.1057	0.3697	0.4382	1.4109	1.4499
0.9	1.0802	1.0747	0.3726	0.4208	1.4117	1.4322

Table 5 presents the accuracy of current model by comparing the numerical results by implementing Tzou and Stehfest algorithms. The results are prepared at $t=0.5$ and $t=1.0$. Both algorithms offer an excellent accuracy of results at both time instants which guaranteed the solution accuracy. Upon increasing the distance from plate, both heat and mass transfer phenomenon reduces. Similarly, the velocity profile enriches when distance from plate increases.

Table 5: Comparative analysis for velocity, temperature and concentration by using Stehfest and Tzou's techniques.

	$T_{(y,t)}$		$C_{(y,t)}$		$V_{(y,t)}$	
	Stehfest Algorithm	Tzou's Algorithm	Stehfest Algorithm	Tzou's Algorithm	Stehfest Algorithm	Tzou's Algorithm
y	$t=0.5$	$t=1.0$	$t=0.5$	$t=1.0$	$t=0.5$	$t=1.0$
0.1	0.0608	0.0610	0.0608	0.0609	0.0748	0.0748
0.2	0.1237	0.1241	0.1237	0.1239	0.1460	0.1461
0.3	0.1910	0.1916	0.1910	0.1913	0.2097	0.2099
0.4	0.2650	0.2658	0.2650	0.2654	0.2619	0.2622
0.5	0.3482	0.3491	0.3482	0.3486	0.2978	0.2981
0.6	0.4434	0.4443	0.4434	0.4439	0.3119	0.3122

6. Conclusions

This study delves into the dynamics of nanofluid MHD flow between two parallel plates, incorporating heat and mass transfer effects within the Prabhakar fractional simulation framework. The significant outcomes of this research are summarized as follows:

- A decrement in temperature profiles with intensification values of fractional parameters have been examined. This trend is indicative of the fractional parameters' role in modulating thermal diffusion within the nanofluid, where higher values appear to impede the thermal transport, leading to lower temperatures across the flow domain.

- The velocity profile demonstrates a direct and positive correlation with the mixed convection parameter. As the mixed convection parameter increases, there is an enhancement in the flow velocity, suggesting that the convective transport is intensified, potentially due to the combined effects of thermal and solutal buoyancy forces.
- An inverse relationship is noted between the velocity of the fluid and the nanoparticle concentration. Higher concentrations of nanoparticles result in a marked decrease in the fluid velocity, which is attributed to the increased effective viscosity.
- The Cu-Water nanofluid showcases a more significant temperature decline when the Prandtl number is increased. This phenomenon is a consequence of copper's higher thermal conductivity, which, when compounded by the Prandtl number effect, results in a more notable temperature drop.
- The velocity profiles show a decrease with an increase in the Prandtl numbers. This is due to the higher Prandtl number enhancing the energy dissipation through conduction, which, reduces the kinetic energy available for the flow, thus decreasing the velocity.
- The concentration profile exhibits a decrement with an increase in the Schmidt number. This behavior underscores the Schmidt number's influence, where higher values signify a relative reduction in mass diffusivity compared to momentum diffusivity, leading to steeper concentration gradients.
- The Al_2O_3 -water nanofluid experiences a more pronounced effect due to changes in the Schmidt number compared to the Cu-Water nanofluid. This is interpreted as the Al_2O_3 nanoparticles impacting the mass transfer properties of the nanofluid more significantly.
- Future recommendations current model may be suggested for utilization of slip effects, Hall applications, porous medium and nonlinear radiated effects. The results can be further modified by performing the entropy generation phenomenon and bioconvective applications.
- The claimed findings present applications in thermal management devices, automotive industries, advanced extrusion systems, chemical reactors, drug delivery systems, and advanced cooling technologies.
- The proposed nanofluid model increases the thermal efficiency by enhancing the heat transfer features, recommended for engineering and industrial applications in manufacturing systems, heat exchangers and power plants. The claimed results optimize the flow behavior subject to different physical constraints like microfluidic systems, lubrication phenomenon and power plants.

Acknowledgment:

This research project was funded by the Deanship of Scientific Research, Princess Nourah bint Abdulrahman University, through the Program of Research Project Funding After Publication, grant No (44- PRFA-P-12).

References

1. F. Bräuer, E. Trautner, J. Hasslberger, P. Cifani, and M. Klein, "Turbulent Bubble-Laden Channel Flow of Power-Law Fluids: A Direct Numerical Simulation Study," *Fluids,* vol. 6, no. 1, p. 40, 2021.

2. S. Kakac, W. Aung, and R. Viskanta, "Natural convection: fundamentals and applications," *Washington,* 1985.

3. A. Singh, H. R. Gholami, and V. Soundalgekar, "Transient free convection flow between two vertical parallel plates," *Heat and mass transfer,* vol. 31, no. 5, pp. 329-331, 1996

4. A. Shafiq, F. Mebarek-Oudina, T. N. Sindhu and Rassoul, G., Sensitivity analysis for Walters' B nanoliquid flow over a radiative Riga surface by RSM, Scientia Iranica, 29 (3), 1236-1249, 2022.

5. M. Narahari, "Transient free convection flow between long vertical parallel plates with ramped wall temperature at one boundary in the presence of thermal radiation and constant mass diffusion," *Meccanica,* vol. 47, no. 8, pp. 1961-1976, 2012.

6. B. K. Jha, B. Aina, and A. Ajiya, "MHD natural convection flow in a vertical parallel plate microchannel," *Ain Shams Engineering Journal,* vol. 6, no. 1, pp. 289-295, 2015.

7. Reddy, B. Prabhakar, A. Jackson Kobia, and M. Paul Matao. "Unsteady mixed convection hydro-magnetic casson thermo-diffusion flow of reacting and dissipating fluid with an inclined magnetic field along an oscillating slanted porous plate." *Computational Thermal Sciences: An International Journal* 16, no. 1 (2024).

8. Cham, Bai Mbye, Shams-ul-Islam Shams-ul-Islam, M. Saleem, Shaiza Talib, and Shafee Ahmad. "Unsteady, two-dimensional magnetohydrodynamic (MHD) analysis of Casson fluid flow in a porous cavity with heated cylindrical obstacles." *AIP advances* 14, no. 4 (2024).

9. Bani-Fwaz, Mutasem Z., Adnan, Sumaira Fayyaz, Nidhish Kumar Mishra, Zafar Mahmood, Sami Ullah Khan, and Muhammad Bilal. "Investigation of unsteady nanofluid over half infinite domain under the action of parametric effects and EPNM." *Journal of Thermal Analysis and Calorimetry* (2024): 1-14.

10. Bhargavi, N., T. Poornima, and Basma Souayeh. "Magnetohydrodynamic conjugate heat transfer analysis on a viscous fluid past a vertical permeable plate." *International Journal of Modern Physics B* 38, no. 16 (2024): 2450211.

11. Warke, A.S., Ramesh, K., Mebarek-Oudina, F. *et al.* Numerical investigation of the stagnation point flow of radiative magnetomicropolar liquid past a heated porous stretching sheet. *J Therm Anal Calorim* 147, 6901–6912 (2022).

12. M. Reddy and S. Shehzad, "Molybdenum disulfide and magnesium oxide nanoparticle performance on micropolar Cattaneo-Christov heat flux model," *Applied Mathematics and Mechanics,* vol. 42, no. 4, pp. 541-552, 2021.

13. Mohsan Hassan, Fateh Mebarek-Oudina, Abrar Faisal, Abdul Ghafar, A.I.Ismail, Thermal energy and mass transport of shear thinning fluid under effects of low to high shear rate viscosity,, International Journal of Thermofluids, Volume 15, August 2022, 100176

14. Balan, Varadhan, Surendran Ramakrishnan, Gopinath Palani, and Mayakannan SELVARAJU. Investigation on the enhancement of heat transfer in counterflow double-pipe heat exchanger using nanofluids, Thermal Science 2024 Volume 28, Issue 1 Part A, Pages: 233-240.

15. Bouzid Kamal, Belarche Lahoucine, Abourida Btissam, Siadi Ali, Nouari Soufiane , Numerical investigation of mixed convection inside a 3-D L-shaped cavity filled with hybrid-nanofluids in the presence of a heating block, Thermal Science, 2024 28(4 Part B):3235-3252

16. Khedher, Nidhal Ben, Zia Ullah, Md Mahbub Alam, Bagh Ali, Saleh Al Arni, Mouldi Ben Amara, and Mohamed Boujelbene. "Significance of fluctuating amplitude and turbulence on

nonlinear radiative heat transfer in Casson nanofluid using primitive and Stokes transformation." *Chaos, Solitons & Fractals* 192 (2025): 116022.

17. Hussain, Muzammil, Bagh Ali, Aziz Ullah Awan, Mohammed Alharthi, and Yasser Alrashedi. "Role of nanoparticle radius for heat transfer optimization in MHD dusty fluid across stretching sheet." *Journal of Thermal Analysis and Calorimetry* 149, no. 24 (2024): 15179-15192.
18. Khan, Shan Ali, Muhammad Imran, Bagh Ali, and Taseer Muhammad. "Towards a new strategy modelling to optimise thermal and solutal transportations within a magnetised blood-based hybrid nanofluid flow over gyrating sphere." *International Journal of Ambient Energy* 46, no. 1 (2025): 2444328.
19. I. Waini, A. Ishak, T. Groşan, and I. Pop, "Mixed convection of a hybrid nanofluid flow along a vertical surface embedded in a porous medium," *International Communications in Heat and Mass Transfer,* vol. 114, p. 104565, 2020.
20. H. Babazadeh, Z. Shah, I. Ullah, P. Kumam, and A. Shafee, "Analysis of hybrid nanofluid behavior within a porous cavity including Lorentz forces and radiation impacts," *Journal of Thermal Analysis and Calorimetry,* vol. 143, no. 2, pp. 1129-1137, 2021.
21. A. Asadi, I. M. Alarifi, and L. K. Foong, "An experimental study on characterization, stability and dynamic viscosity of CuO-TiO2/water hybrid nanofluid," *Journal of Molecular Liquids,* vol. 307, p. 112987, 2020.
22. G. Huminic and A. Huminic, "Entropy generation of nanofluid and hybrid nanofluid flow in thermal systems: a review," *Journal of Molecular Liquids,* vol. 302, p. 112533, 2020.
23. S. Nadeem, N. Abbas, and M. Malik, "Inspection of hybrid based nanofluid flow over a curved surface," *Computer Methods and Programs in Biomedicine,* vol. 189, p. 105193, 2020.
24. Ying-Qing Song, M. Ijaz Khan, Sumaira Qayyum, R. J. Punith Gowda, R. Naveen Kumar, B. C. Prasannakumara, Yasser Elmasry and Yu-Ming Chu, Physical impact of thermo-diffusion and diffusion-thermo on Marangoni convective flow of hybrid nanofluid ($MnZiFe_2O_4$–$NiZnFe_2O_4$–H_2O) with nonlinear heat source/sink and radiative heat flux, Modern Physics Letters BVol. 35, No. 22, 2141006 (2021).
25. Ying-Qing Song, Aamir Hamid, Tian-Chuan Sun, M. Ijaz Khan, Sumaira Qayyum, R. Naveen Kumar, , B. C. Prasannakumara, Sami Ullah Khan, Ronnason Chinram, Unsteady mixed convection flow of magneto-Williamson nanofluid due to stretched cylinder with significant non-uniform heat source/sink features , Alexandria Engineering Journal, Volume 61, Issue 1, January 2022, Pages 195-206.
26. R. S. Varun Kumar, R. J. Punith Gowda, R. Naveen Kumar, M. Radhika & B. C. Prasannakumara, Two-phase flow of dusty fluid with suspended hybrid nanoparticles over a stretching cylinder with modified Fourier heat flux, SN Applied Sciences volume 3, Article number: 384 (2021)
27. B.C.Prasannakumara, Numerical simulation of heat transport in Maxwell nanofluid flow over a stretching sheet considering magnetic dipole effect, Partial Differential Equations in Applied Mathematics, Volume 4, December 2021, 100064
28. Mulupuri Nagapavani, Venkat Rao Kanuri, Mohammed Fareeduddin, K. Thanesh Kumar, Uma C. Kolli, M. Sunitha, Chetana Gali, Rangaswamy Naveen KumarFeatures of the exponential form of internal heat generation, Cattaneo–Christov heat theory on water-based

graphene–CNT–titanium ternary hybrid nanofluid flow, Heat Transfer, Volume52, Issue1, January 2023, Pages 144-161

29. B. Mahanthesh, Statistical and Exact Analysis of MHD Flow Due to Hybrid Nanoparticles Suspended in C2H6O2-H2O Hybrid Base Fluid, 9780429343537, CRC Press, (2020).

30. Mackolil, J., Mahanthesh, B. Time-Dependent Nonlinear Convective Flow and Radiative Heat Transfer of Cu-Al_2O_3-H_2O Hybrid Nanoliquid with Polar Particles Suspension: a Statistical and Exact Analysis. BioNanoSci. 9, 937–951 (2019).

31. Sheikholeslami, M., Z. Khalili, Fatemeh Salehi, and Ladan Momayez. "Simulation of sustainable solar thermal storage system involving photovoltaic panel equipped with nanofluid-based splitter considering self-cleaning coating." *Sustainable Cities and Society* 119 (2025): 106100.

32. Mezaache, Abderrahmane, Fateh Mebarek-Oudinal, Hanumesh Vaidya, and Katta Ramesh. "Impact of nanofluids and porous structures on the thermal efficiency of wavy channel heat exchanger." *International Journal of Thermal Sciences* 210 (2025): 109673.

33. J. Gómez-Aguilar, H. Yépez-Martínez, R. Escobar-Jiménez, C. Astorga-Zaragoza, L. Morales-Mendoza, and M. González-Lee, "Universal character of the fractional space-time electromagnetic waves in dielectric media," *Journal of Electromagnetic Waves and Applications,* vol. 29, no. 6, pp. 727-740, 2015.

34. M. Duarte Ortigueira and J. Tenreiro Machado, "Fractional derivatives: The perspective of system theory," *Mathematics,* vol. 7, no. 2, p. 150, 2019.

35. Turkyilmazoglu, Mustafa. "Hyperthermia therapy of cancerous tumor sitting in breast via analytical fractional model." *Computers in Biology and Medicine* 164 (2023): 107271.

36. Turkyilmazoglu, Mustafa, and Mohamed Altanji. "Fractional models of falling object with linear and quadratic frictional forces considering Caputo derivative." *Chaos, Solitons & Fractals* 166 (2023): 112980.

37. Ibraheem, Ghada H., Mustafa Turkyilmazoglu, and M. A. Al-Jawary. "Novel approximate solution for fractional differential equations by the optimal variational iteration method, *Journal of Computational Science* 64 (2022): 101841.

38. Turkyilmazoglu, Mustafa, and Mohamed Altanji. "Fractional models of falling object with linear and quadratic frictional forces considering Caputo derivative." *Chaos, Solitons & Fractals* 166 (2023): 112980.

39. N. Sene, "Second-grade fluid model with Caputo–Liouville generalized fractional derivative," *Chaos, Solitons & Fractals,* vol. 133, p. 109631, 2020.

40. M. Mozafarifard and D. Toghraie, "Time-fractional subdiffusion model for thin metal films under femtosecond laser pulses based on Caputo fractional derivative to examine anomalous diffusion process," *International Journal of Heat and Mass Transfer,* vol. 153, p. 119592, 2020.

41. Asjad Muhammad Imran, Zahid Muhammad, Chu Yu-Ming, Baleanu Dumitru, Prabhakar fractional derivative and its applications in the transport phenomena containing nanoparticles, Thermal Science 2021 Volume 25, Issue Spec. issue 2, Pages: 411-416

42. Asjad, M.I., Muhammad Danish Ikram, Ali Ahmadian, Soheil Salahshour & Mehdi Salimi, New solutions of generalized MHD viscous fluid flow with thermal memory and bioconvection. J Therm Anal Calorim 147, 14019–14029 (2022).

43. Sarwar, N.; Asjad, M.I.; Sitthiwirattham, T.; Patanarapeelert, N.; Muhammad, T. A Prabhakar Fractional Approach for the Convection Flow of Casson Fluid Across an Oscillating Surface Based on the Generalized Fourier Law . Symmetry 2021, 13, 2039.

44. Muhammad Imran Asjad, Pongsakorn Sunthrayuth, Muhammad Danish Ikram, Taseer Muhammad, Ali Saleh Alshomrani Analysis of non-singular fractional bioconvection and thermal memory with generalized Mittag-Leffler kernel, Chaos, Solitons & Fractals, Volume 159, June 2022, 112090

45. A. Giusti and I. Colombaro, "Prabhakar-like fractional viscoelasticity," *Communications in Nonlinear Science and Numerical Simulation,* vol. 56, pp. 138-143, 2018.

46. A. Akgül and I. Siddique, "Novel applications of the magnetohydrodynamics couple stress fluid flows between two plates with fractal-fractional derivatives," *Numerical Methods for Partial Differential Equations,* vol. 37, no. 3, pp. 2178-2189, 2021.

47. F. Wang, M. I. Asjad, M. Zahid, A. Iqbal, H. Ahmad, and M. Alsulami, "Unsteady thermal transport flow of Casson nanofluids with generalized Mittag–Leffler kernel of Prabhakar's type," *Journal of materials research and technology,* vol. 14, pp. 1292-1300, 2021.

48. A. Raza, H. A. Hejazi, S. U. Khan, M. I. Khan, K. Smida, and I. Tlili, "Unsteady incompressible flow of magnetized aluminium oxide and titanium oxide nanoparticles with blood base fluid," *Journal of the Indian Chemical Society,* p. 100568, 2022.

49. Khalid Abdulkhaliq M. Alharbi, Ibrahim B. Mansir, Kamel Al-Khaled, M. Ijaz Khan, Ali Raza, Sami Ullah Khan, Mohamed Ayadi & M. Y. Malik, "Heat transfer enhancement for slip flow of single-walled and multi-walled carbon nanotubes due to linear inclined surface by using modified Prabhakar fractional approach," *Archive of Applied Mechanics,* pp. 1-11, 2022.

Nomenclature

Symbol	Quantity	Symbol	Quantity
U	Velocity component (m/s)	Gr	Heat Grashof number
t	Times (s)	T_d	Ambient temperature (K)
g	Gravity acceleration (m/s^2)	α, β, γ	Prabhakar Fractional parameters
k_{nf}	Thermal conductivity (W/mk)	Sc	Schmidt number
C_f	Skin friction	M	Magnetic field
ρ_{nf}	Nanofluid density (Kg/m^3)	q	Laplace transform variable
U_0	Characteristic velocity(ms^{-1})	B_o	Magnetic field strength (Kg/s^2)
θ	The angle of magnetic inclination	C_p	Specific heat (J/kgK)
Gm	Mass Grashof number	Pr_{eff}	Prandtl number
μ_{nf}	Dynamic viscosity (Kg/ms)	T_w	Wall temperature (K)
β_T	Thermal expansion coefficient	σ	Electrical conductivity
Nu	Nusselt number	Sh	Sherwood number

Submitted: 03.12.2024.

Revised: 06.03.2025.

Accepted: 10.03.2025.